Eur. Phys. J. D **15**, 145–154 (2001)

THE EUROPEAN PHYSICAL JOURNAL D

EDP Sciences

Recombination of U^{92+} ions with electrons

W. Shi[1], S. Böhm[1], C. Böhme[1], C. Brandau[1], A. Hoffknecht[1], S. Kieslich[1], S. Schippers[1], A. Müller[1,a], C. Kozhuharov[2], F. Bosch[2], B. Franzke[2], P.H. Mokler[2], M. Steck[2], Th. Stöhlker[2], and Z. Stachura[3]

[1] Institut für Kernphysik, Justus-Liebig-Universität, 35392 Giessen, Germany
[2] Gesellschaft für Schwerionenforschung (GSI), 64291 Darmstadt, Germany
[3] Institute for Nuclear Physics, 31-342 Kraków, Poland

Received 1st March 2001 and Received in final form 20 April 2001

Abstract. Recombination of fully stripped U^{92+} ions with electrons has been investigated at the Experimental Storage Ring (ESR) in Darmstadt. Absolute recombination rate coefficients have been measured for relative energies from 0 to 33 eV. For energies greater than 20 meV the experimental result is well described by the theory for radiative recombination (RR). Below 20 meV the experimental rate increasingly exceeds the RR calculation as observed previously in the recombination of light bare ions as well as of Bi^{83+}. This low-energy rate enhancement is shown to scale as $Z^{2.6}$ for bare ions, where Z is the atomic number of the ion. The U^{92+} recombination rate enhancement is insensitive to changes of the electron density. Variation of the magnetic guiding field strength from 80 mT to 120 mT resulted in oscillations of the recombination rate at 0 eV. The oscillations are partly attributed to changes of the transverse electron temperature accompanying the change of the magnetic guiding field strength; partly they may be caused by uncompensated small changes of the interaction angle between the two beams.

PACS. 34.80.Lx Electron-ion recombination and electron attachment – 29.20.Dh Storage rings

1 Introduction

Recombination of an electron with a highly charged ion is a fundamental process of great importance. It provides an excellent testing ground for atomic collision theory. Cross-sections and rate coefficients of recombination processes are needed for the understanding of astrophysical and fusion plasmas. Moreover, low-energy electron-ion recombination with its large cross-section provides a very promising scheme for the production of anti-hydrogen by recombination of positrons with antiprotons [1].

For bare ions the main recombination mechanism is radiative recombination (RR), in which a free electron is captured by an ion A^{q+} and the excess energy and momentum are carried away by a photon:

$$e^- + A^{q+} \rightarrow A^{(q-1)+} + \gamma. \quad (1)$$

Another recombination mechanism possible for bare ions is three-body recombination (TBR), where the excess energy and momentum are carried away by a second electron:

$$A^{q+} + e^- + e^- \rightarrow A^{(q-1)+} + e^-. \quad (2)$$

This process is important at high electron densities and low collision energies.

After the pioneering experiment on recombination of bare ions performed by Andersen *et al.* [2] for C^{6+} in 1990, consecutive measurements for bare ions (He^{2+}, C^{6+}, N^{7+}, Ne^{10+}, Si^{14+}, Cl^{17+}, Ar^{18+}) [3–9] have been carried out. The measured rate coefficients have been in agreement with RR theory for relative energies greater than 0.1 eV, or even already 0.01 eV. However, while Andersen *et al.* measured recombination rates at (seemingly) zero center-of-mass energy which were only slightly below theory, all other measurements found recombination rates exceeding theoretical predictions at very low relative energies ($E_{\rm rel} \leq 0.01$ eV). Towards lower energies the measured rate coefficient $\alpha_{\rm exp}$ typically shows an extra amount $\Delta\alpha = \alpha_{\rm exp} - \alpha_{\rm RR}$ on top of the theoretical rate coefficient $\alpha_{\rm RR}$ for RR. The resulting rate enhancement factor $\epsilon = \alpha_{\rm exp}/\alpha_{\rm RR}$ at $E_{\rm rel} = 0$ eV increases from 1.6 (He^{2+}) to 10 (Ar^{18+}); enhancement was observed recently also with D^+ [10].

Historically, recombination rate enhancement was observed first in 1989 in the recombination of U^{28+} [11]. This finding stimulated continuous efforts in the investigation of RR of bare ions as well as of multicharged ions. Whereas the very high rate enhancement of multicharged complex ions like Au^{25+}, Au^{50+}, Pb^{53+} and U^{28+} could be partly traced back to the presence of additional recombination channels, *i.e.*, mainly due to dielectronic recombination (DR) [12–15], the origin of the remaining discrepancies between experiment and theory especially for bare

[a] e-mail: Alfred.Mueller@strz.uni-giessen.de

ions, where DR cannot occur, is not understood. Theoretically a number of mechanisms have been proposed [16–21]. However, none of these has been successful in providing a satisfactory explanation of the enhancement so far.

Experimental efforts to understand the rate enhancement concentrated on investigating the influence of individual experimental parameters. Variations of the electron density [7–9] within a total range from about 10^6 cm^{-3} up to 10^{10} cm^{-3} did not show effects on the enhancement. The excess recombination rate $\Delta\alpha$ was found to scale with transverse electron temperature as $T_\perp^{-1/2}$ and with longitudinal electron temperature as $T_\parallel^{-1/2}$ [8]. A systematic study of the ion charge-state dependence of the excess rate for a number of light bare ions [4] yielded a $Z^{2.8}$ scaling for atomic numbers $1 \leq Z \leq 14$. Another external parameter observed to influence the enhancement has been the magnetic guiding field B in the interaction region. An increase of the excess rate at 0 eV with increasing magnetic field strength has been found in a number of experiments, *e.g.*, references [8,12,22]. In these experiments an approximate B^x scaling ($0.5 \leq x \leq 1$) for the excess rate was found.

Recently, the investigations have been extended to the heaviest bare ions [23], in which relativistic and QED effects play a role. In the recombination of Bi^{83+} [23], an enhancement factor as high as 5.2 was found. Besides that, the low-energy recombination rates were found to oscillate almost periodically with the magnetic guiding field strength. Surprisingly, this kind of oscillations have not been observed in the experiment for Bi^{80+}, which was carried out in the same beam time but with a three times lower ion energy, *i.e.*, 100 MeV/u.

Here we present experimental results for recombination of U^{92+}, which is the heaviest bare ion accessible to detailed recombination experiments. The recombination rate coefficient was measured in a wide energy range covering many orders of magnitude (between the lowest energy meaningful in this experiment, 10^{-5} eV all the way up to 30 eV). The influence of the magnetic guiding field strength and electron density on the rate enhancement has been investigated in great detail. In comparison with the previous study for Bi^{83+}, new features have been implemented in the experiment. Mainly, the two-dimensional ion-beam profile was probed simultaneously with the recombination spectra. This provides a direct additional observation channel for monitoring the ion-beam location and size which is useful for the interpretation of the recombination data.

2 Theory

In order to describe RR Kramers developed a semi-classical approach already in 1923 [24]. A full quantum mechanical treatment within the non-relativistic dipole approximation was performed by Stobbe seven years later [25]. In 1957, Bethe and Salpeter [26] derived from a quantum mechanical approach an approximate formula for the RR cross-section, which is identical to Kramers' semi-classical result

$$\sigma_{\mathrm{RR}}(n, E_{\mathrm{cm}}) = \sigma_0 \frac{E_0^2}{nE_{\mathrm{cm}}(E_0 + n^2 E_{\mathrm{cm}})} \tag{3}$$

with $\sigma_0 \approx 2.1 \times 10^{-22}$ cm^2. The capture of an electron by a bare ion produces a hydrogenic state with principal quantum number n. In this case $E_0 = Z^2\mathcal{R}$ is the binding energy of the ground state electron in the hydrogenic ion (atom) with nuclear charge Z and Rydberg constant $\mathcal{R} \approx 13.6$ eV, and E_{cm} is the kinetic energy in the electron-ion c.m. frame. The total cross-section for this process is obtained by summing up the contributions of all accessible Rydberg states:

$$\sigma_{\mathrm{RR}}(E_{\mathrm{cm}}) = \sum_{n=1}^{n_{\max}} \sigma_{\mathrm{RR}}(n, E_{\mathrm{cm}}), \tag{4}$$

where $n_{\max}$ is the maximum principal quantum number of the Rydberg states that can contribute. This number is determined by the experimental conditions. As a semi-classical approximation equation (3) is only valid in the limit of high quantum numbers and low electron energies. Since the quantum mechanical treatment of Stobbe involves rather tedious evaluation of hydrogenic dipole matrix elements one often applies correction factors $G_n(E_{\mathrm{cm}})$, the so-called Gaunt factors, to equation (3) to account for deviations from the correct quantum result at low n and high E_{cm}. The use of Gaunt factors is convenient because they are either tabulated [27] or given in an easy parameterization [28,29]. We here apply tabulated [30] values $k_n = G_n(0)$ and use

$$\sigma_{\mathrm{RR}}(E_{\mathrm{cm}}) = \sigma_0 \sum_{n=1}^{n_{\max}} k_n \frac{(Z^2\mathcal{R})^2}{nE_{\mathrm{cm}}(Z^2\mathcal{R} + n^2 E_{\mathrm{cm}})} \cdot \tag{5}$$

This Gaunt-factor corrected calculation differs by as much as $\sim$ 20% (see Fig. 1a) from the uncorrected one (*cf.* Eq. (4)).

For very heavy ions an exact relativistic calculation within the framework of Dirac theory and with the inclusion of higher multipoles is demanded in general. Results of such calculations for bare ions with $n \leq 3$ have recently been presented by Ichihara and Eichler [31]. When comparing their result for U^{92+} with the outcome of equation (5) with $Z = 92$ and $n_{\max} = 3$ we find that over the energy range covered in the present experiment the maximum difference is less than 3% (*cf.* Fig. 1a). This is due to cancellation effects as shown in Figure 1b where the contributions by each individual n are plotted separately. The differences between the relativistic and non-relativistic calculations change sign when going from $n = 1$ to $n = 2$. The absolute difference is largest for $n = 1$ (up to $\sim$ 10%). In general, relativistic effects become weaker with increasing n. Therefore, we do not expect the difference to increase when extending the summation to higher principal quantum numbers. Since the 3% maximum deviation of the n-summed non-relativistic calculation from the fully relativistic calculation is smaller than the experimental

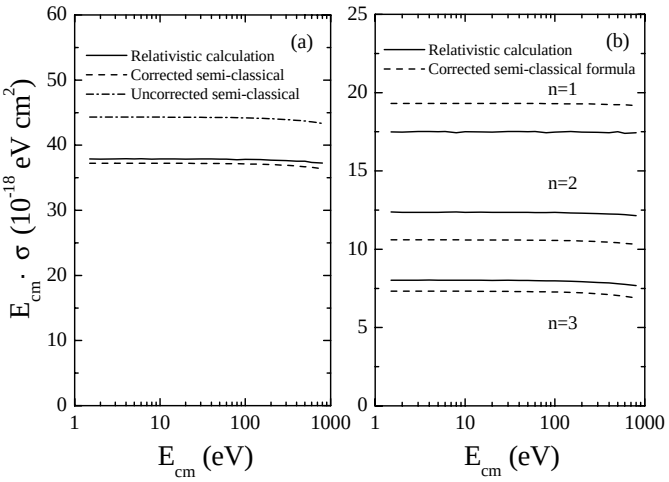

Fig. 1. Theoretical cross-sections for radiative recombination of bare U^{92+} ions as a function of the relative energy. (a) Comparison between n-summed ($n_{\max} = 3$) fully relativistic [31] (full line), semi-classical Gaunt-factor corrected (*cf.* Eq. (5)) (dashed line) and uncorrected (*cf.* Eq. (4)) (dash-dotted line) calculations. In order to remove the divergence at $E_{\rm cm} = 0$ the cross-sections have been multiplied by $E_{\rm cm}$. (b) n-selective comparison between fully relativistic (full line) and Gaunt-factor corrected semi-classical (*cf.* Eq. (5)) (dashed line) calculations for $n = 1$, 2, 3 individual shells.

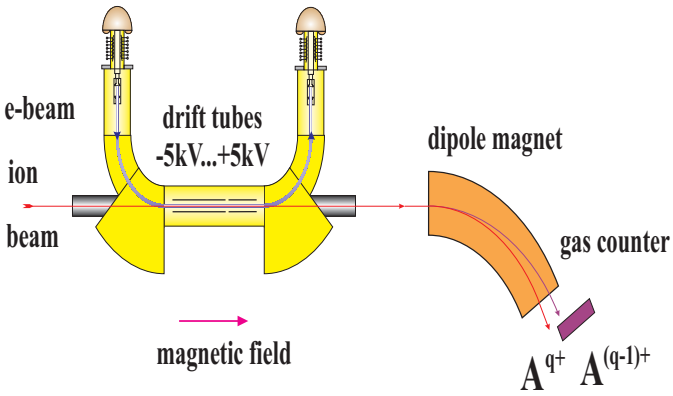

Fig. 2. Schematic view of the ESR electron cooler and a conceptual view of the experimental set-up for recombination measurements. The cold electron beam produced in the gun is guided by the magnetic field and merged with the ion beam over a distance of 2.5 m. The electron beam is then separated from the ion beam by the magnetic guiding field and transferred to the collector. Recombined and parent ions are separated from each other in the dipole magnets after the cooler. A gas counter detector located about 50 m downstream from the electron cooler is used to detect the recombined ions.

uncertainty, equation (5) was used for all calculations presented in this paper. QED corrections to the cross-section for radiative capture into the $n = 1$ shell of bare uranium have recently been calculated by Shabaev *et al.* [32]. They amount to less than 1% at the highest energy considered and are therefore neglected here.

For comparison with the experimental results a theoretical rate coefficient $\alpha_{\rm RR}$ is derived by a convolution of the theoretical RR cross-section $\sigma_{\rm RR}$ (*cf.* Eq. (5)) with a velocity distribution function $f(v_{\rm rel}, \mathbf{v})$

$$\alpha_{\rm RR}(v_{\rm rel}) = \int \sigma_{\rm RR}(v) v f(v_{\rm rel}, \mathbf{v}) \mathrm{d}^3 v. \qquad (6)$$

The average longitudinal c.m. velocity $v_{\rm rel}$ can be calculated from

$$v_{\rm rel} = |v_{\rm e,||} - v_{\rm i,||}|/(1 - v_{\rm i,||} v_{\rm e,||}/c^2), \qquad (7)$$

where $v_{\rm e,\|}$ and $v_{\rm i,\|}$ are the longitudinal velocity components of the electrons and ions in the laboratory frame, respectively. The anisotropic velocity distribution $f(v_{\rm rel}, \mathbf{v})$ is given by

$$f(v_{\rm rel}, \mathbf{v}) = \frac{m_{\rm e}}{2\pi k T_\perp} \exp\left(-\frac{m_{\rm e} v_\perp^2}{2kT_\perp}\right) \times \sqrt{\frac{m_{\rm e}}{2\pi k T_\|}} \exp\left(-\frac{m_{\rm e}(v_\| - v_{\rm rel})^2}{2kT_\|}\right), \qquad (8)$$

where $v_\|$ is the velocity component in the beam direction, $v_\perp$ the velocity component perpendicular to the beam, and $T_\|$ and $T_\perp$ are temperatures characterizing the distributions of relative velocities between electrons and ions in the longitudinal and transverse directions, respectively.

3 Experiment

The main features of the experimental technique have been described previously [23]. The measurement has been performed at the Experimental Storage Ring (ESR) of the Gesellschaft für Schwerionenforschung (GSI) in Darmstadt. 291.7 MeV/u U^{92+} ions supplied by the GSI linear accelerator UNILAC in combination with the heavy ion synchrotron SIS were injected into the ESR. One injection pulse of ions from the SIS into the ESR was sufficient to provide an ion current of typically 300–500 μA (corresponding to $1.1-1.9 \times 10^7$ ions stored in the ring) at the beginning of a measurement. In one of the straight sections of the storage ring the ion beam was merged with the magnetically confined electron beam of the cooler (see Fig. 2). The electron energy was set to 160 keV at cooling so that the electron and ion mean velocities were identical. Under these conditions the ion beam is cooled by friction forces exerted by the electron beam on ions whose velocity does not match the velocity of the cold electron beam. By elastic electron-ion collisions energy is lost by ions which are faster than the electrons and energy is gained by ions which are slower until, ideally, the ion beam has acquired the low temperature of the electron beam and the average velocities of electrons and ions are fully matched. Dipole magnets after the electron cooler bent the circulating U^{92+} ion beam onto a closed orbit and separated the recombined U^{91+} ions from the circulating U^{92+} ions. The recombined U^{91+} ions were detected by a gas counter detector, which is located in the north part of the ESR, *i.e.* downstream more than half way around the ring.

Before starting a measurement, the ion beam was cooled for several seconds until the beam profiles reached their equilibrium widths. For a change of the electron energy voltages between -5 and 5 kV were applied to two

drift tubes surrounding the electron and ion beams in the interaction region. During a measurement cycle the electron energy was stepped through a preset range of values different from the cooling energy thus introducing non-zero mean relative velocities between the ions and the electrons. In between two measurement steps of 30 ms duration each, the electron energy was set to the cooling energy ($E_{\rm rel} = 0$) for 30 ms in order to maintain good ion-beam quality. The experimental data stream was continuously collected and stored each ms, thus allowing a detailed off-line analysis. The recombined-ion-beam profile was probed with a two-dimensional position-sensitive multi-wire gas counter and recorded in the data stream. This new feature made possible to monitor the ion-beam location and size simultaneously with the recombination measurements. The time-resolved measurements allowed us to check for possible effects of the friction force between the electrons and the ions, which tends to shift the relative energy between electrons and ions to a value lower than the set value. Such effects have, in fact, not been observed in the present study as well as in the previous study on Bi^{83+}. This is in agreement with a detailed simulation of the influence of the friction force.

The kinetic energy of the electrons $E_{\rm e}$ is defined by the cathode voltage $U_{\rm gun}$, the drift tube voltage $U_{\rm drift}$ and the space charge potential $U_{\rm sp}$ in the interaction region:

$$\begin{aligned} E_{\rm e} &= -eU_{\rm gun} + eU_{\rm drift} + eU_{\rm sp} \\ &= -eU_{\rm gun} + eU_{\rm drift} - \frac{I_{\rm e} r_{\rm e} m_{\rm e} c^2}{e v_{\rm e}} \left[1 + 2\ln(b/a)\right], \end{aligned} \quad (9)$$

where e, $m_{\rm e}$ and $v_{\rm e}$ are the electron charge, mass and velocity, $r_{\rm e}$ the classical electron radius, c the speed of light, $I_{\rm e}$ the electron current, $b = 10$ cm and $a = 2.54$ cm are the radii of the drift tube and the electron beam, respectively. The ion-beam diameter in the interaction region is only of the order of a millimeter and, hence, the electron energy distribution probed by the ions is rather flat across the ion beam. For a typical electron current $I_{\rm e} = 80$ mA the space charge potential on the drift tube axis is $U_{\rm sp} = -13.8$ V at cooling, *i.e.* for $U_{\rm gun} = -160$ kV and $U_{\rm drift} = 0$. The electron energy $E_{\rm cool}$ at cooling, *i.e.* for $E_{\rm rel} = 0$ (*cf.* Eq. (10)), directly determines the ion energy $E_{\rm i} = (m_{\rm i}/m_{\rm e})E_{\rm cool}$.

The space-charge corrected electron energy $E_{\rm e}$ and ion energy $E_{\rm i}$ are used to calculate the relative energy $E_{\rm rel}$ between the electron and the ion:

$$\begin{aligned} E_{\rm rel} &= \mu c^2 \left[\gamma_{\rm i}\gamma_{\rm e} - \sqrt{(\gamma_{\rm i}^2 - 1)(\gamma_{\rm e}^2 - 1)}\cos(\theta) - 1\right], \\ \mu &= \frac{m_{\rm e} m_{\rm i}}{(m_{\rm e} + m_{\rm i})}, \\ \gamma_{\rm e} &= 1 + \frac{E_{\rm e}}{m_{\rm e} c^2}, \\ \gamma_{\rm i} &= 1 + \frac{E_{\rm i}}{m_{\rm i} c^2}, \end{aligned} \quad (10)$$

where $m_{\rm i}$ is the mass of the ion, and θ is the angle between the electron and the ion beams. This formula for the relative energy calculation is valid as long as $E_{\rm rel} \ll \sqrt{2 m_{\rm i} c^2 m_{\rm e} c^2}$, which is always satisfied in recombination experiments. For "normal" recombination measurements the alignment of the beams was optimized to $\theta = 0$ mrad with an uncertainty of 0.1 mrad by minimizing the width of the ion beam. This width was observed by a beam-profile monitor based on the detection of secondary ions produced by the circulating beam in the residual gas. Alternatively, the position-sensitive detection of fast ions that dropped out of the circulating beam after electron capture from the residual gas provided a measure of the beam width.

The counting rate measured at the scanning energy $E_{\rm meas}$ is given by

$$R(E_{\rm meas}) = \frac{\alpha(E_{\rm meas})\eta L n_{\rm e}(E_{\rm meas}) N_{\rm i}}{C\gamma^2} + R_{\rm back}, \quad (11)$$

with α denoting the electron-ion recombination rate coefficient, η the detection efficiency of the recombination detector which is very close to unity, $L = 2.5$ m the nominal length of the interaction zone, $n_{\rm e}(E)$ the electron density at energy E, $N_{\rm i}$ the number of stored ions, $C = 108.36$ m the ring circumference and γ the relativistic Lorentz factor for the transformation between the c.m. and the laboratory frames. $R_{\rm back}$ denotes the measured background rate due to collisions with residual gas molecules. In order to extract an absolute rate coefficient from the experimental data the background has to be subtracted by taking into account the counting rate at a reference energy $E_{\rm ref}$

$$R(E_{\rm ref}) = \frac{\alpha(E_{\rm ref})\eta L n_{\rm e}(E_{\rm ref}) N_{\rm i}}{C\gamma^2} + R_{\rm back}. \quad (12)$$

Combining equations (11, 12) α at $E_{\rm meas}$ is calculated from

$$\begin{aligned} \alpha(E_{\rm meas}) = {} & \frac{[R(E_{\rm meas}) - R(E_{\rm ref})] C\gamma^2}{\eta L n_{\rm e}(E_{\rm meas}) N_{\rm i}} \\ & + \alpha(E_{\rm ref}) \frac{n_{\rm e}(E_{\rm ref})}{n_{\rm e}(E_{\rm meas})}. \end{aligned} \quad (13)$$

In the present experiment the reference energy has been set to the maximum accessible scan energy, *i.e.*, at $E_{\rm ref} = 33$ eV. According to RR theory the rate coefficient at this energy is $\alpha(E_{\rm ref}) = 1.0 \times 10^{-9}$ cm^3 s^{-1}.

Electron and ion beams were merged and demerged by bending the electron beam in and out of the ion-beam direction using toroidal magnetic fields with a bending radius of 120 cm. The electron beam of 2.54 cm radius is still overlapping the ion beam for 25 cm before and after the straight overlap section of 250 cm. The merging and demerging sections therefore contribute to the measured counting rate. However, the influence of the voltage applied to the drift tubes is restricted to the straight overlap section of the cooler and thus, the electron energy in the toroidal sections is always the same, independent of the drift tube potential. Therefore the contribution of the merging and demerging sections can be treated as an electron-energy-independent background.

The electrons strictly follow the magnetic field lines. Nonzero angles between the electron trajectory and the

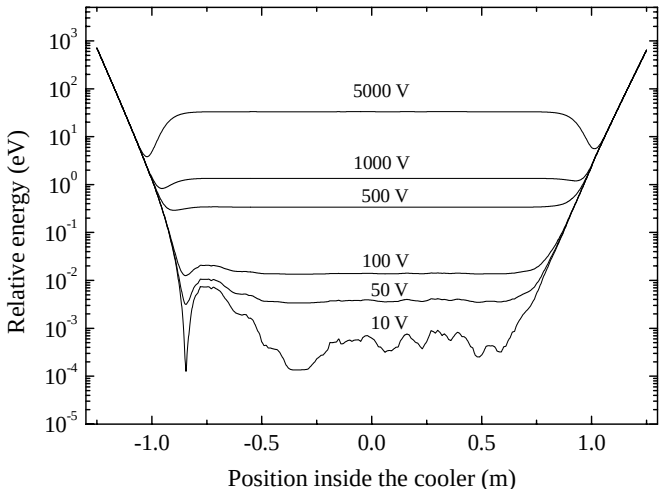

Fig. 3. Relative energies between electrons and ions along the straight overlap section inside the ESR cooler resulting from the drift tube electric potential and the interaction-angle distributions. The voltages of 10, 50, 100, 500, 1000 and 5000 V applied to the drift tubes correspond to $E_{\rm rel} = 6.2 \times 10^{-4}$, 0.0039, 0.014, 0.34, 1.35 and 33.2 eV, respectively. Position 0 represents the middle of the drift tube.

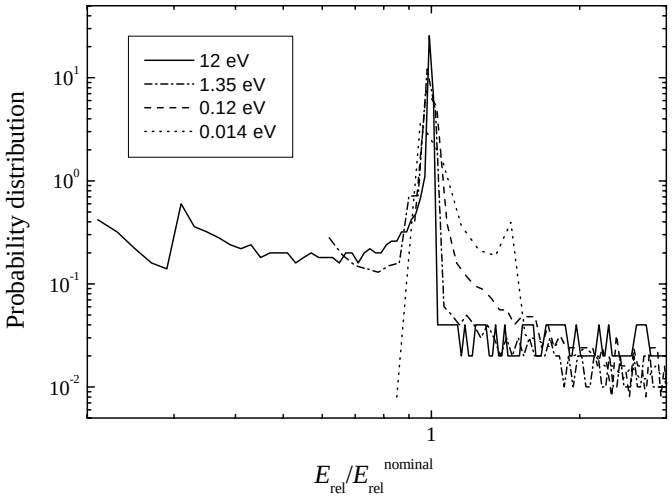

Fig. 4. Probability distribution of relative energies experienced in the cooler at a few sample nominal (desired) energies $E_{\rm rel}^{\rm nominal}$. Dotted line represents distribution at 0.014 eV nominal energy; dashed line at 0.12 eV; dash-dotted line at 1.35 eV; solid line at 12.0 eV. The area under each curve is normalized to unity.

ion-beam direction along the cooler geometrical axis are introduced by the transverse components of the magnetic guiding field in the merging section. Figure 3 shows the resulting relative energies along the straight overlap section for sample voltages applied to the drift tubes. Consequently the desired energy can only be realized with a certain energy-dependent probability (see Fig. 4) or, in other words, over a certain energy-dependent fraction of the whole interaction length. Thus, the measured rate coefficient at a given nominal relative energy $E_{\rm meas}$ contains contributions from other relative energies; *i.e.*, it results from the convolution

$$\alpha(E_{\rm meas}) = \frac{1}{L}\int_0^L {\rm d}l\, \alpha(E_{\rm rel}(l)), \qquad (14)$$

with $E_{\rm rel}(l)$ being the relative energy at the position l inside the cooler. The real rate coefficient $\alpha(E_{\rm rel}(l))$ can therefore be obtained by a deconvolution performed iteratively. The numerical procedure is described in reference [23].

The systematic uncertainty of the experimental rate coefficients is estimated to be ±15% based on the possible error in the ion-current and electron-current measurements and the uncertainty of the drift tube potential and angle distributions. Concerning the uncertainty of the relative energies, at higher energies, *e.g.*, 10 eV, it comes mainly from the error in the drift tube voltage measurement. It amounts to about 0.06 eV. At lower energies, it is determined mainly by the uncertainty of the interaction angle between the two beams. The upper limit of the possible error is about 2 meV if an uncertainty of 0.1 mrad is assumed for the interaction angle. Experiment suggests that the error of the relative energies due to possible misalignment of the beams at lower energies (up to $E_{\rm rel} = 20$ meV) is no more than 0.1 meV.

4 Experimental results and discussion

4.1 Comparison with theory

In Figure 5 the measured absolute recombination rate coefficient of U^{92+} is plotted *versus* the relative energy from 0 to 33 eV. For comparison, rate coefficients calculated with equations (5, 6, 8) are also shown in the figure.

The highest Rydberg state $n_{\rm max}$ that can contribute to the measured rate in experiments using storage rings is determined by field ionization in the dipole magnet which separates the parent ions and the recombined ions. The field-ionization limit $n_{\rm F}$ is determined [33] by

$$n_{\rm F} = \left(7.3 \times 10^{10}\ {\rm V/m} \times \frac{q^3}{F}\right)^{1/4}, \qquad (15)$$

where q is the charge state of the ion and $F = v_{\rm i,\|} B_\perp$ the motional electric field seen by the ions with velocity $v_{\rm i,\|}$ in the transverse magnetic field $B_\perp$ of the charge-analyzing magnet. Practically, one has to take into account also higher Rydberg states which can radiatively decay to states below $n_{\rm F}$ before their arrival at the analyzing magnet. Calculations based on a detailed model [34] for field ionization and cascading of Rydberg states formed in recombination shows that $n_{\rm max} = 130$ is a realistic estimate for U^{92+}. Consequently, the value is used for the calculations throughout the rest of this paper.

As seen from Figure 5a very good agreement between the calculated and measured recombination rate coefficients is found for energies greater than 20 meV. Towards lower energies up to 0.1 meV the measured rate is increasingly greater than the calculated value and becomes flat

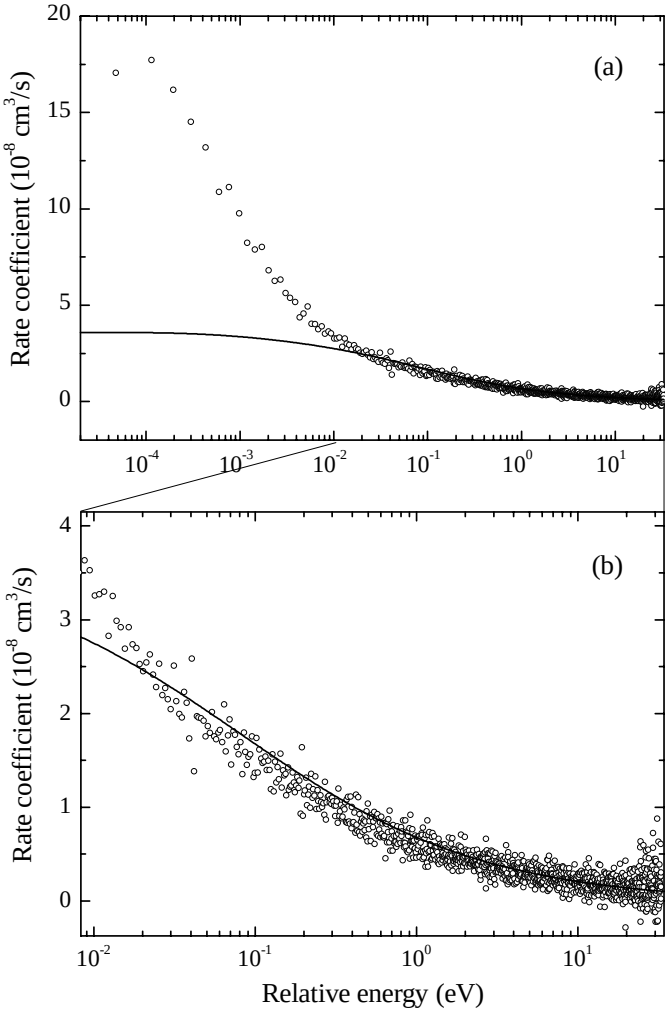

Fig. 5. Absolute recombination rate coefficients of U^{92+} plotted against relative energy between the electron and the ion. Open circles represent measured results; lines the calculated results. (a) An overview of the whole energy range; (b) detailed comparison for energies greater than 1×10^{-2} eV. The solid line (a, b) is a calculation with $n_{\max} = 130$, $kT_{\perp} = 120$ meV and $kT_{\parallel}$=0.1 meV. The magnetic guiding field strength was 104 mT.

below 0.1 meV. This is known as low-energy rate enhancement as mentioned in the introduction. Obviously the size of the enhanced rate is energy dependent. At 0 eV the rate coefficient amounts to 1.8×10^{-7} cm^3 s^{-1} exceeding the theoretical value of 3.6×10^{-8} cm^3 s^{-1} by a factor of 5. The scattering of the data points in the recombination spectrum originates from the deconvolution procedure as well as from the limited counting statistics particularly in the higher energy region.

4.2 Variation of the magnetic guiding field strength

Motivated by previous surprising findings in the recombination of Bi^{83+} [23], recombination rates at 0 eV have been measured with variation of the magnetic guiding field

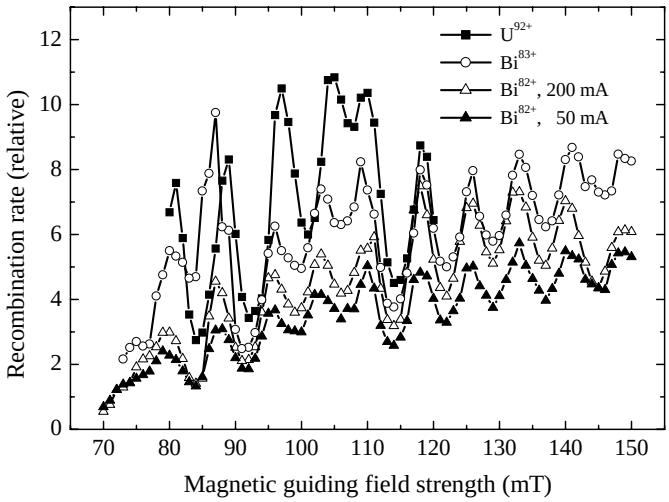

Fig. 6. Recombination rates at 0 eV of U^{92+}, Bi^{83+} [23] and Bi^{82+} for different magnetic guiding field strengths. The recombination rates were evaluated from the counting rate of the recombined ions without any background subtraction and corrections due to the drift tube potential and angle distributions inside the cooler. The difference of the recombination rates for Bi^{82+} measured with different electron currents are mainly due to incomplete normalization of backgrounds originating from collisions with residual gas molecules in the ion beam path.

strength. Data were taken for magnetic field strengths $B_{\parallel}$ between 80 mT and 120 mT in steps of 1 mT and the results are shown in Figure 6. Also shown in the figure are results for Bi^{82+} and for Bi^{83+}. As for Bi^{83+}, the rates for U^{92+} and Bi^{82+} oscillate with the magnetic field strength. It is striking that the recombination rates for the different ions measured in different beam times react to the change of the magnetic guiding field strength with a similar behaviour. In particular the positions (magnetic field strength) of the maxima and minima of the oscillations coincide. This indicates that besides possible pure effects of the magnetic field on the recombination process, the magnetic guiding field may have influenced the properties (*e.g.* temperatures) of the electron beam inside the cooler consistently in a periodic manner, which in turn affects the recombination process.

In order to further investigate this experimental phenomenon, complete recombination spectra at 15 selected magnetic field strengths between 80 mT and 110 mT were measured. Sample spectra at four different magnetic guiding field strengths are given in Figure 7. In these recombination spectra the measured rate coefficients are essentially identical for energies greater than 1 eV irrespective of the magnetic field strength. At lower energies, however, pronounced differences exist. Comparison of the measured spectra with RR theory facilitates the extraction of the transverse temperatures characterizing the velocity distribution. Although the shape of the recombination spectrum is rather insensitive to even order-of-magnitude variations of the longitudinal temperature, the apparent transverse temperature can be determined rather uniquely

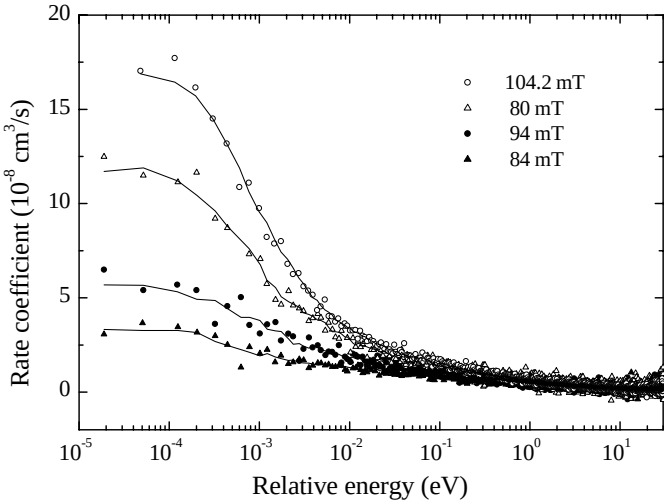

Fig. 7. Recombination spectra of U^{92+} measured at four different magnetic guiding field strengths. Full circles at 94 mT; triangles at 80 mT; full triangles 84 at mT; open circles at 104.2 mT. To guide the eye, smooth curves are drawn through the data points.

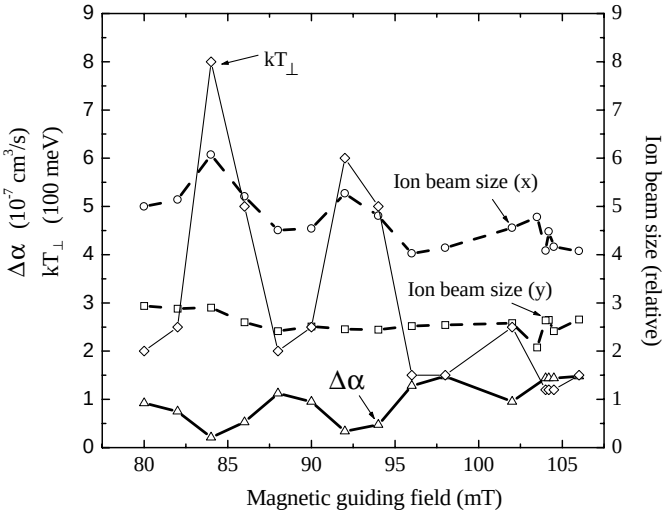

Fig. 8. Excess recombination rate $\Delta\alpha$ at 0 eV of U^{92+}, transverse temperature $kT_\perp$ and ion-beam sizes in horizontal (x) and vertical (y) directions plotted against the magnetic guiding field strength. Triangles represent $\Delta\alpha$; diamonds show the $kT_\perp$ invoked to reproduce the energy dependence of measured recombination rates at energies above $\approx 5 \times 10^{-2}$ eV; open circles represent the measured ion-beam size in the horizontal direction; open squares the ion-beam size in the vertical direction. Different from Figure 6, $\Delta\alpha$ values are based here on complete recombination spectra with corrections for background and the distribution of relative energies along the axis of the cooler. The quantities $kT_\perp$ have been determined individually by comparing each recombination spectrum with RR theory. The ion-beam size is defined as 2σ of the beam-profile distribution. To guide the eye, data points are connected with different sorts of lines.

(with an estimated error of $\pm 20\%$) from the comparison between experiment and theory for energies greater than 0.02 eV. In this energy range the rate enhancement does not appear, and RR theory agrees with the experiment. At the low energies a decreasing transverse temperature leads to increased enhancement (see [8]).

In Figure 8 the excess rates $\Delta\alpha$ at 0 eV together with the transverse temperature $kT_\perp$ and ion beam sizes in horizontal (x) and vertical (y) directions are plotted against the magnetic guiding field strength. The quantities $\Delta\alpha$, $kT_\perp$ and the ion-beam size d_x in the horizontal direction oscillate with identical periods. Thereby $\Delta\alpha$ exhibits a 180 degree phase difference as compared to the other two quantities. In contrast to d_x, the ion beam size d_y in the vertical direction does not oscillate. We note that the change of the apparent transverse temperature with magnetic guiding field strength is related to the change of the ion-beam size.

It is known that the excess rate and $T_\perp$ are interrelated. To remove the established $(kT_\perp)^{-1/2}$ dependence [8], scaled excess rates $\Delta\alpha(kT_\perp)^{1/2}$ are plotted in Figure 9 against the magnetic guiding field strength. The dependence of the scaled excess rate on the magnetic field strength is much smoother than the excess rate itself as expected. The ratio between the maximum and minimum scaled excess rate is about 3, whereas for the unscaled rate the ratio amounts to 7.

There appears three possibilities that may explain the remaining oscillation behaviour and the general trend of increasing recombination rate observed for increasing magnetic guiding field. One possibility is a variation not only of $T_\perp$ but also of $T_\parallel$. Assuming that the remaining oscillation of $\Delta\alpha(kT_\perp)^{1/2}$ is due to oscillation of $T_\parallel$ and considering the known $T_\parallel^{-1/2}$ dependence of $\Delta\alpha$, one would have to assume a variation of $T_\parallel$ by up to a factor

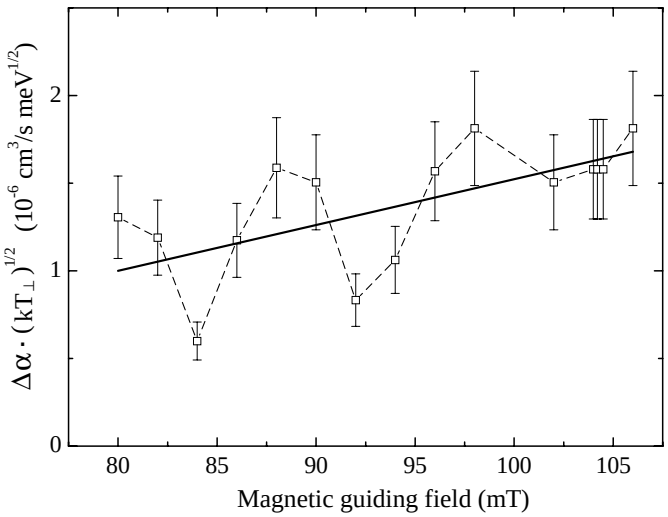

Fig. 9. Scaled excess rate $\Delta\alpha(kT_\perp)^{1/2}$ at 0 eV of U^{92+} as a function of the magnetic guiding field strength. The quoted error $\pm 18\%$ includes contributions from $\Delta\alpha$ and $kT_\perp$. To guide the eye, data points are connected with dashed lines, a straight solid line is drawn to show the gross trend of the magnetic field dependence.

of 9. Unfortunately, the complete energy-dependent recombination rate measurements such as those displayed in Figure 7 cannot provide conclusive information on $T_\parallel$ (as is possible for $T_\perp$) because the RR rate is insensitive to order-of-magnitude variations of $T_\parallel$. Direct measurement of the temperatures by low energy DR resonances is desirable, but no isolated resonances at sufficiently low relative energy have been found in very heavy ions accessible at ESR so far.

The second possible reason for the oscillatory behaviour of the scaled excess rate could be a real magnetic-field effect. The fact that the oscillations are almost identical for completely different experiments with U^{92+}, Bi^{83+}, and Bi^{82+} with different settings of ring parameters supports the assumption of a periodic dependence of recombination on the magnetic guiding field. However, as noted already in the introduction the oscillations have not been observed in recombination experiments at lower ion energies (corresponding to lower cooling energies).

A third parameter that influences the recombination rate and might be changed when the magnetic field is varied is the angle between the ion beam and the electron beam. By increasing the magnetic guiding field strength the trajectories of the electrons can be expected to change only little, however, the ion beam – though having a high rigidity – is bent sideways as the toroidal field in the cooler is increased. Since this bending was not compensated in the experiment one has to expect a change of the angle θ between the ion-beam and the electron-beam axis. When θ increases from 0 to 0.2 mrad the lowest accessible relative energy between the electrons and ions increases to $E_{\rm rel}^{\rm min}(\theta = 0.2\ {\rm mrad}) = 0.0074$ eV. Keeping this in mind in combination with the very rapid decrease of the recombination rate when the relative energy is detuned from 0 eV, a variation of θ between 0 and 0.15 mrad would reproduce the observed remaining oscillations of the recombination rate. If this scenario were the only explanation it would not at all be clear why this effect – the angular variation – should be periodic with $B_\parallel$.

The above discussion shows that none of the three explanations is really satisfying without further knowledge. What remains is that with increasing magnetic guiding field strength the average recombination rate at the lowest relative energy also increases (see solid line in Fig. 9). This increase almost resembles a linear dependence of $\Delta\alpha(kT_\perp)^{1/2}$ with $B_\parallel$.

4.3 Variation of the electron density

Recombination measurements with electron densities of 6.3×10^5 cm^{-3} (40 mA) and 1.3×10^6 cm^{-3} (80 mA) were carried out. The shapes of these two recombination spectra are slightly different for the energy range from 20 meV to 1 eV where rate enhancement is not expected. This difference seems to indicate slightly different transverse temperatures at electron densities which differ by a factor of 2. Transverse temperatures of 250 meV and 200 meV were evaluated for the velocity distributions at the two different densities by comparing the measured and calculated rate coefficients for energies above 20 meV. The excess rates at 0 eV for the densities 6.3×10^5 cm^{-3} and 1.3×10^6 cm^{-3} are slightly different, being 6.5×10^{-8} cm^3 s^{-1} and 7.8×10^{-8} cm^3 s^{-1} respectively. However, the scaled excess rates $\Delta\alpha(kT_\perp)^{1/2}$ are identical. In agreement with previous findings in recombination experiments performed with a variety of ions at different facilities, no significant influence of the electron density on the rate enhancement was found in the present study as well. The lack of electron-density dependence of the rate enhancement rules out TBR (Eq. (2)) as a possible mechanism leading to enhanced recombination rates at low energies. The TBR mechanism would suggest a linear dependence of the enhanced rates on the electron density.

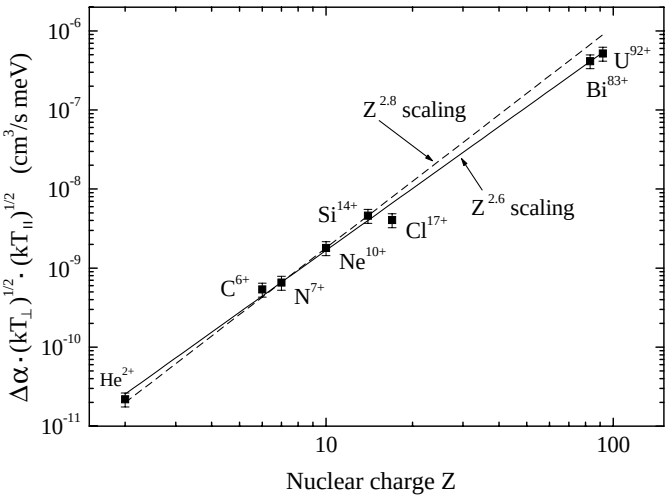

Fig. 10. Nuclear charge dependence of the scaled excess rates $\Delta\alpha(kT_\perp)^{1/2}(kT_\parallel)^{1/2}$ at 0 eV in the recombination of fully stripped ions. All experiments for fully stripped ions utilizing storage rings [3,4,7–9,23] are included. $\Delta\alpha(kT_\perp)^{1/2}(kT_\parallel)^{1/2}$ values are based on $kT_\perp$ and $kT_\parallel$ quoted in the respective papers. These excess rates have not been normalized to the same magnetic guiding field strength. The magnetic field was 30 mT for He^{2+}, N^{7+}, Ne^{10+} and Si^{14+}, 42 mT for C^{6+}, 63 mT for Cl^{17+}, 110 mT for Bi^{83+}, and 104 mT for U^{92+}. An uncertainty of 20% is assumed for all scaled excess rates, mainly because of possible uncertainty in the transverse and longitudinal electron temperatures. Full squares are experimental results; dashed line is a $Z^{2.8}$ scaling found previously by Gao *et al.* [4] in the recombination of light ions; solid line is a $Z^{2.6}$ new scaling based on all data points plotted here.

4.4 Nuclear charge dependence

In order to provide an overview of the low-energy rate enhancement in the recombination of fully stripped ions, scaled excess recombination rates at 0 eV of ions from all available experiments performed with ion storage rings have been plotted in Figure 10. We can see from the figure that the rate enhancement of the U^{92+} ion as well as that of the Bi^{83+} ion essentially agree with the $Z^{2.8}$ scaling behaviour found in the recombination of light ions [4]. However, a new fit based on all the data points

plotted in Figure 10 yields a slightly different scaling with $\Delta\alpha(kT_\perp)^{1/2}(kT_\parallel)^{1/2} \propto Z^{2.6}$. We note that the $Z^{2.6}$ scaling for the rate enhancement $\Delta\alpha(kT_\perp)^{1/2}(kT_\parallel)^{1/2}$ is beyond the Z^2 scaling behaviour expected for the radiative recombination rate $\sigma_{\rm RR}$.

5 Conclusions

The recombination of U^{92+} ions with free electrons has been studied experimentally. Absolute recombination rate coefficients have been measured for relative energies from 0 to 33 eV. Comparison of the experimental recombination rate coefficients with available RR theory shows good agreement for relative energies greater than 20 meV. At lower energies the well known rate enhancement appears also in the recombination of U^{92+}. New evaluation of the nuclear charge dependence of the rate enhancement at 0 eV results in a $Z^{2.6}$ scaling, which is valid for both light and the heaviest bare ions. As in the recombination of other ions the size of the rate enhancement does not depend on the electron density. This rules out TBR as a possible mechanism leading to enhanced recombination rates at low energies.

The present investigation shows that the oscillation of the recombination rate at 0 eV with the magnetic guiding field strength observed in the present experiment as well as in the previous experiment with Bi^{83+} can partly be explained by a change of the transverse electron temperature accompanying the change of the magnetic guiding field strength. The remaining dependence may be explained by variations of the longitudinal temperature and possible variations of the interaction angle. Averaging over the oscillations yields an increase of the rate enhancement $\Delta\alpha(kT_\perp)^{1/2}$ by a factor of 1.7 when the magnetic guiding field strength is increased from 80 mT to 105 mT.

Finally, we point out that a capture-state-selective measurement of radiative recombination would provide a more stringent test of theories for radiative recombination, particularly of those for very heavy ions where relativistic effects need to be taken into account. A photon-and-recombined-ion coincidence measurement of the recombination can distinguish RR from TBR as well as from dielectronic recombination (DR) in the case of not fully stripped ions and thus may lead to a better understanding of the low-energy enhancement in the recombination of bare ions and in particular of multicharged ions. Such experiments are currently under consideration.

The Giessen group gratefully acknowledges support for this work through contracts GI MÜL S and GI-MÜ2 with the Gesellschaft für Schwerionenforschung (GSI), Darmstadt, and by research grants (numbers 06 GI 848 and 06 GI 947) from the Bundesministerium für Bildung und Forschung (BMBF), Bonn.

References

1. M. Holzscheiter, M. Charlton, Rep. Prog. Phys. **62**, 1 (1999).
2. L.H. Andersen, J. Bolko, P. Kvistgaard, Phys. Rev. Lett. **64**, 729 (1990).
3. H. Gao, D.R. DeWitt, R. Schuch, W. Zong, S. Asp, M. Pajek, Phys. Rev. Lett. **75**, 4381 (1995).
4. H. Gao, R. Schuch, W. Zong, E. Justiniano, D.R. DeWitt, H. Lebius, W. Spies, J. Phys. B **30**, L499 (1997).
5. A. Wolf, J. Berger, M. Bock, D. Habs, B. Hochadel, G. Kilgus, G. Neureither, U. Schramm, D. Schwalm, W. Szmola, A. Müller, M. Wagner, R. Schuch, Z. Phys. D Suppl. **21**, S69 (1991).
6. O. Uwira, A. Müller, W. Spies, A. Frank, J. Linkemann, C. Brandau, T. Cramer, C. Kozhuharov, J. Klabunde, N. Angert, P.H. Mokler, R. Becker, M. Kleinod, N.R. Badnell, Hyperf. Interact. **108**, 167 (1997).
7. H. Gao, S. Asp, C. Biedermann, D.R. DeWitt, R. Schuch, W. Zong, H. Danared, Hyperf. Interact. **99**, 301 (1996).
8. G. Gwinner, A. Hoffknecht, T. Bartsch, M. Beutelspacher, N. Eklöw, P. Glans, M. Grieser, S. Krohn, E. Lindroth, A. Müller, A.A. Saghiri, S. Schippers, U. Schramm, D. Schwalm, M. Tokman, G. Wissler, A. Wolf, Phys. Rev. Lett. **84**, 4822 (2000).
9. A. Hoffknecht, S. Schippers, A. Müller, G. Gwinner, D. Schwalm, A. Wolf, Phys. Scripta (in print).
10. N. Eklöw, S. Madzunkov, T. Mohamed, R. Schuch, W. Zong, P. Glans, H. Danared, in Manne Siegbahn Laboratory Annual Report 1999, edited by A. Källberg, E. Oppenheimer (Manne Siegbahn Laboratory, Stockholm, 2000), p. 75.
11. A. Müller, S. Schennach, M. Wagner, J. Haselbauer, O. Uwira, W. Spies, E. Jennewein, R. Becker, M. Kleinod, U. Pröbstel, N. Angert, J. Klabunde, P.H. Mokler, P. Spädtke, B. Wolf, Phys. Scripta T **37**, 62 (1991).
12. A. Hoffknecht, O. Uwira, S. Schennach, A. Frank, J. Haselbauer, W. Spies, N. Angert, P.H. Mokler, R. Becker, M. Kleinod, S. Schippers, A. Müller, J. Phys. B **31**, 2415 (1998).
13. O. Uwira, A. Müller, J. Linkemann, T. Bartsch, C. Brandau, M. Schmitt, A. Wolf, D. Schwalm, R. Schuch, W. Zong, H. Lebius, W.G. Graham, J. Doerfert, D.W. Savin, Hyperf. Interact. **108**, 149 (1997).
14. S. Baird, J. Bosser, C. Carli, M. Chanel, P. Levèvre, R. Ley, R. Maccaferri, S. Maury, I. Meshkov, D. Möhl, G. Molinari, F. Motsch, H. Mulder, G. Tranquille, F. Varenne, Phys. Lett. B **361**, 184 (1995).
15. G.F. Gribakin, A.A. Gribakina, V.V. Flambaum, Aust. J. Phys. **52**, 443 (1999).
16. L. Bureyeva, V. Lisitsa, J. Phys. B **31**, 1477 (1998).
17. M. Pajek, R. Schuch, Hyperf. Interact. **108**, 185 (1997).
18. Y. Hahn, P. Krstić, J. Phys. B **27**, L509 (1994).
19. Y. Hahn, J. Li, Z. Phys. D **36**, 85 (1996).
20. G. Zwicknagel, C. Toepffer, P.G. Reinhard, Laser Part. Beams **13**, 311 (1995); Hyperf. Interact. **99**, 285 (1996).
21. Q. Spreiter, C. Toepffer, Hyperf. Interact. **114**, 245 (1998); J. Phys. B **33**, 2347 (2000).
22. A. Hoffknecht, T. Bartsch, S. Schippers, A. Müller, N. Eklöw, P. Glans, M. Beutelspacher, M. Grieser, G. Gwinner, A.A. Saghiri, A. Wolf, Phys. Scripta T **80**, 298 (1999).

23. A. Hoffknecht, C. Brandau, T. Bartsch, C. Böhme, H. Knopp, S. Schippers, A. Müller, C. Kozhuharov, K. Beckert, F. Bosch, B. Franzke, A. Krämer, P.H. Mokler, F. Nolden, M. Steck, Th. Stöhlker, Z. Stachura, Phys. Rev. A **63**, 012702 (2001).
24. H.A. Kramers, Philos. Mag. **46**, 836 (1923).
25. M. Stobbe, Ann. Physik **7**, 661 (1930).
26. H.A. Bethe, E.E. Salpeter, *Quantum Mechanics of One- and Two-Electron Systems* (Springer, Berlin, Heidelberg, New York, 1957).
27. K. Omidvar, P.T. Guimaraes, Astrophys. J. Suppl. **73**, 555 (1990).
28. M.R. Flannery, in *Atomic, Molecular & Optical Physics Handbook* (American Institute of Physics, New York, 1996), p. 625.
29. E. Zerrad, Y. Hahn, J. Quant. Spectrosc. Radiat. Transfer **59**, 637 (1998).
30. L.H. Andersen, J. Bolko, Phys. Rev. A **42**, 1184 (1990).
31. A. Ichihara, J. Eichler, At. Data Nucl. Data Tab. **74**, 1 (2000).
32. V.M. Shabaev, Y.A. Yerokhin, T. Beier, J. Eichler, Phys. Rev. A **61**, 052112 (2000).
33. A. Müller, D.S. Belić, B.D. DePaola, N. Djurić, G.H. Dunn, D.W. Mueller, C. Timmer, Phys. Rev. A **36**, 599 (1987).
34. S. Schippers, A. Müller, G. Gwinner, J. Linkemann, A.A. Saghiri, A. Wolf, Astrophys. J. **555**, (in print, 2001).